International Journal of Heat and Mass Transfer 130 (2019) 1–8

Contents lists available at ScienceDirect

International Journal of Heat and Mass Transfer

journal homepage: www.elsevier.com/locate/ijhmt

Modeling a thermoplate conical heat exchanger in a point focus solar thermal collector

Imane Khalil *, Quinn Pratt, Christopher Spitler, Daniel Codd

Shiley-Marcos School of Engineering – University of San Diego, San Diego, CA 92110, United States

ARTICLE INFO

Article history:
Received 14 August 2018
Received in revised form 8 October 2018
Accepted 8 October 2018

Keywords:
Computational fluid dynamics
Heat exchanger design
FLUENT
Solar thermal receiver
CSP
Dimpleplate

ABSTRACT

A three-dimensional ANSYS-FLUENT Computational Fluid Dynamics (CFD) model of the central receiver in a compact hybrid solar-thermal collector is presented. The small scale cavity receiver is conical in shape, laser welded from Inconel 625 with a 38 mm entrance aperture, and uses pressurized water as the Heat Transfer Fluid (HTF) within a thermoplate serpentine flowpath. The coupled thermofluidic CFD model examines a simplified unrolled version of this dimpleplate heat exchanger, representing the laminar flow within 10 × 1 mm expanded flowpath serpentine channels complete with intrachannel spot welds and non-uniform concentrated solar irradiance heating. The computational model is validated against experimental results with the receiver at the focus of a 2.7 m^2 parabolic dish, two-axis tracking rooftop solar collector. For steady state conditions with the outlet HTF reaching temperatures in excess of 200 °C, the HTF temperature rise predicted by the computational model is in agreement with the experimental data. In order to accurately capture the heat losses from the heat exchanger to its surrounding, we present an additional three-dimensional CFD model including the heat exchanger and surrounding thermal insulation. Contours of temperature and velocity at the midplane of the dimpleplate receiver heat exchanger are presented.

1. Introduction

The hybrid photovoltaic-solar thermal (PV/T) method of energy production combines the conversion of solar radiation to electricity through photovoltaic (PV) cells and the harnessing of solar heat to drive a traditional heat-engine or for industrial process heating. The appeal of the hybrid PV/T design is to increase overall system efficiency by converting more of the solar energy spectrum into usable energy [1,2].

The apparatus in this study uses a paraboloidal mirror to concentrate sunlight onto a hybrid collector at the focal point. This design is intended to generate electricity both through concentrated photovoltaic (CPV) and concentrated solar power (CSP).

A receiver assembly is positioned at the focal point of the concentrating mirror. The receiver assembly consists of a spectrum splitting, transmissive coarse PV array which absorbs in the ultraviolet and visible range [3,4]. Spillage, bypass, and infrared light will pass through the PV array and be captured by a Thermal Receiver (TR). A rooftop PV/T testbed was constructed to investigate this design as a scaleable source for renewable energy.

This work focuses on modeling only the thermal receiver and comparisons to TR-only receiver experimental data, operated for medium temperature process heat needs (i.e. T < 250 °C). Studies on this system's PV-related components can be found in [3,5].

We construct two full-scale three-dimensional CFD models for the TR system using the commercial package ANSYS®, FLUENT, Release 18.0. The first model details the formed nickle alloy serpentine thermoplate channel with water as the working fluid. The second model was used to approximate heat losses to the environment.

First we provide details of the TR model including methods for modeling losses in the system. Second we discuss the solar concentrator testbed and the operating conditions during the experiment used for the TR model validation. Third, we present results from the TR model.

2. Hybrid concentrator apparatus

The rooftop testbed, shown in Fig. 1, consists of a two-axis sun tracker, 2.72 m^2 concentrating mirror, receiver assembly, and the receiver support arm. The testbed uses a heat transfer fluid (HTF) feed system that supplies water at a controlled pressure and flowrate to the thermal receiver.

* Corresponding author.
E-mail addresses: ikhalil@sandiego.edu (I. Khalil), quinnpratt@sandiego.edu (Q. Pratt), cspitler@sandiego.edu (C. Spitler), codd@sandiego.edu (D. Codd).

https://doi.org/10.1016/j.ijheatmasstransfer.2018.10.041
0017-9310/

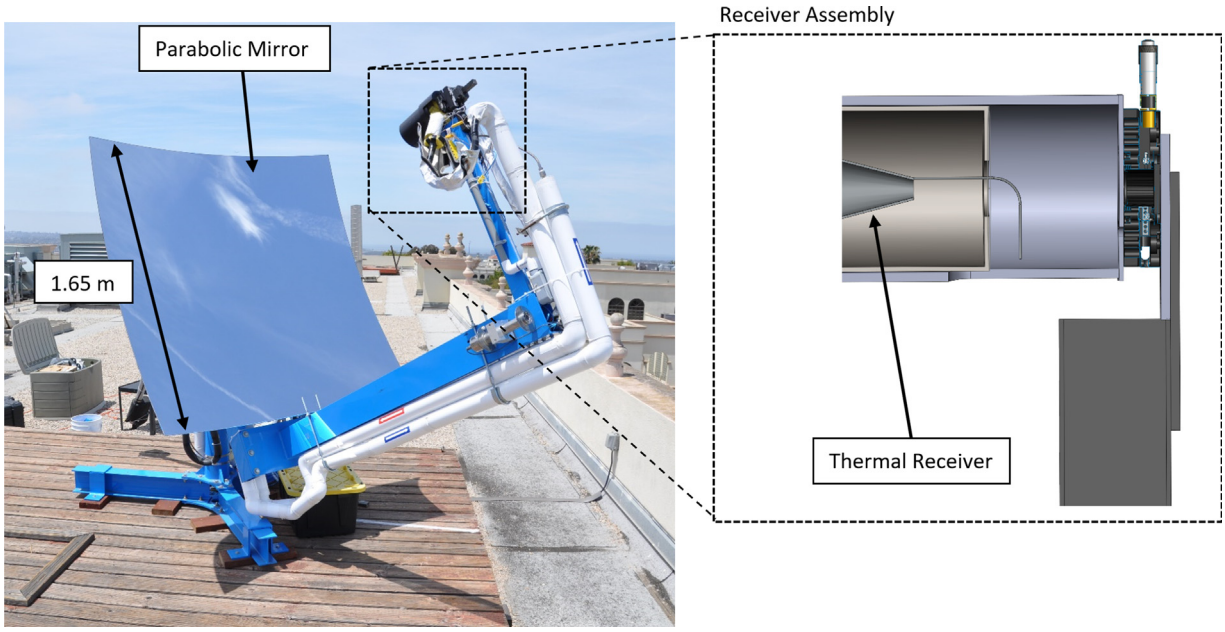

Fig. 1. Photograph of the rooftop solar collector and schematic cross-section of the receiver assembly.

The Receiver Assembly, also shown in Fig. 1, contains two primary components: the Thermal Receiver, and the PV array. This report is exclusively concerned with modeling the Thermal Receiver alone. The PV array is removed for the present experiment.

The mass flow rate through the TR is controlled with a positive displacement metering pump with adjustable stroke and measured using an Omega FLR1009ST-D flowmeter. An adjustable pressure relief valve downstream of the TR sets the pressure of the fluid at the outlet of the receiver.

For the experiment presented in this work, the working fluid of the thermal receiver is water. Due to the high operating temperature, the thermal receiver was held at a gauge pressure of 19 bar to ensure single phase flow.

Fluid pressures were measured at the inlet and outlet of the TR using Omega PX119-1KAI pressure transducers. Temperatures at the fluid centerline of the inlet and outlet pipes were measured using type K thermocouples.

Environmental conditions including the ambient temperature and wind speed were also recorded. An Eppley NIP normal incidence pyrheliometer mounted to the two-axis tracker records the direct normal irradiance (DNI) of incoming sunlight, measured in W/m^2.

The experiment achieved steady-state conditions for 3 h, during which the mass flowrate was recorded as $\dot{m} = 1.1 \pm 0.1$ g/s. The ambient temperature was $T_\infty = 21.9 \pm 0.7$ °C and the inlet temperature was $T_{in} = 33.0 \pm 0.3$ °C; the HTF outlet temperature was 206.5 ± 1.8 °C. The DNI was recorded as $\overline{\text{DNI}} = 971.6 \pm 5.4$ W/m^2 and the wind speed was $\overline{u} = 1.8 \pm 0.8$ m/s.

3. CFD modeling

3.1. Thermal receiver model

The TR, shown in Fig. 2(a), is constructed using two seam-welded sheets of 0.5 mm Inconel-625. The welded sheets are rolled into a cone and the long edges are welded together. The cone has dimensions: 38 mm entrance inner diameter, 50 mm axial length and 12 mm exit inner diameter.

The cone is then placed in a fixture and hydraulically inflated to a target fluid-channel height of 1.0 mm. The serpentine fluid path features spot-welds along the fluid direction. The spot-welds, or 'dimples', were needed for structural integrity and found to improve the overall heat transfer in previous work [6].

The cavity surrounding the TR is packed with high-temperature mineral wool insulation when it is installed in the receiver assembly. The fluid pipes are also wrapped with closed-cell silicone insulation. The inside wall is coated with Pyromark 2500 Paint for enhanced solar absorptivity and reduced emissivity [7].

The inflated 'dimpleplate' geometry of the thermal receiver is complex, making it difficult to model accurately. Several approximations were made to simplify the geometry. First, the conical cavity is modeled in the un-rolled state as shown in Fig. 2(b).

For the TR used in this experiment the inflation procedure was asymmetric about the mid-plane resulting in a predominately flat outside wall. Therefore, only the inside wall of the model possesses the full-3D curvature.

The Inconel sheets are modeled as part of the geometry in order to capture conduction between neighbouring arcs of the serpentine path. Fig. 3 shows the geometry of the 3D FLUENT model of the TR. The computational mesh contains approximately 2.8 million elements. Calculations were performed in parallel on the University of San Diego's High Performance Computing Cluster (HPCC). Clock time was on the order of 10 min.

The fluid is expected to experience a large temperature change. In order to accurately capture the fluid behavior, the properties of water are set to vary in FLUENT as a function of temperature according to the IAPWS-97 formulation [8].

Reynolds number is calculated using,

$$\text{Re} = \frac{4\dot{m}}{\pi D_H \mu}. \tag{1}$$

with an effective hydraulic diameter, D_H, of 2.0 mm, laminar interior channel flow is expected in the majority of the computational domain with Re < 2300. FLUENT is used to solve the following equations inside the thermal receiver:

The continuity equation,

$$\frac{\partial \rho}{\partial t} + \nabla \cdot \left(\rho \vec{U}\right) = 0, \tag{2}$$

the momentum equation,

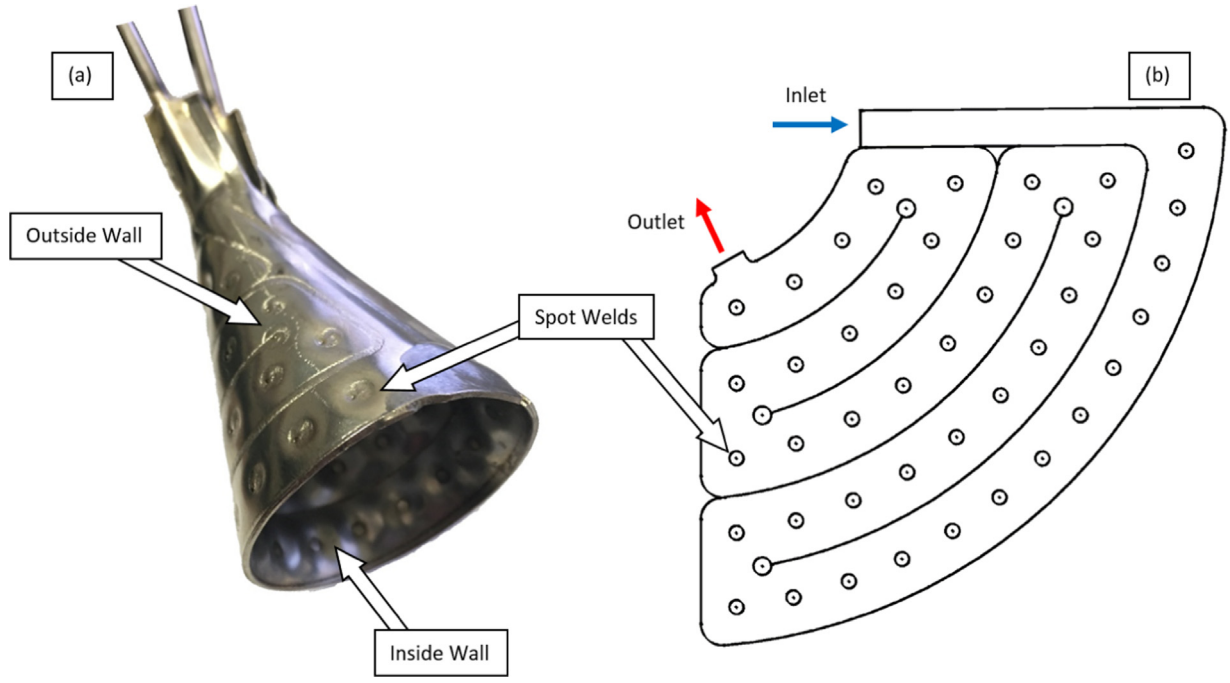

Fig. 2. (a) photograph of the conical thermal receiver. (b) schematic of the un-rolled TR illustrating the flow-path.

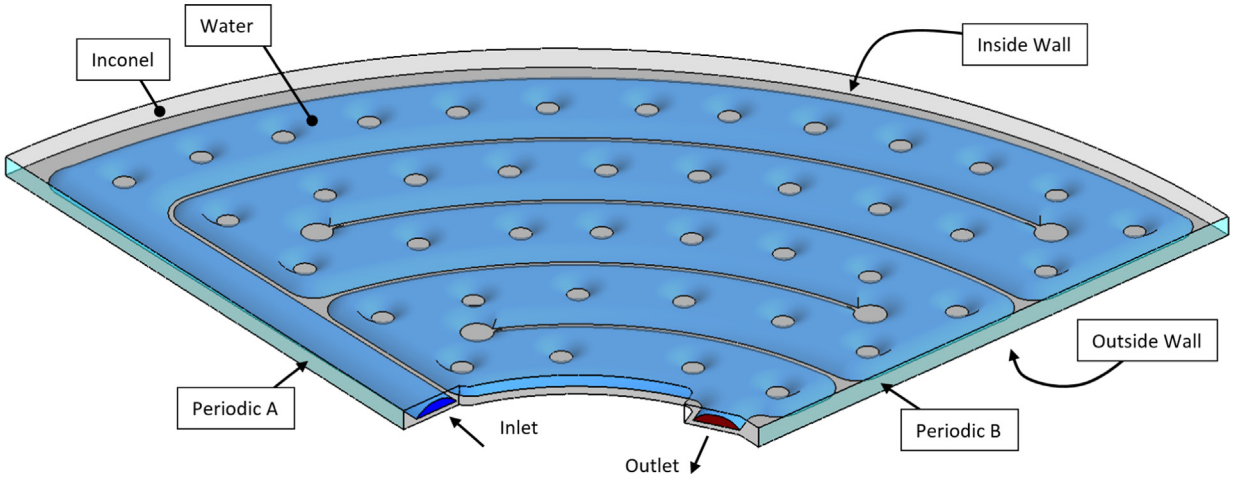

Fig. 3. Boundary conditions of the TR FLUENT model.

$$\frac{\partial}{\partial t}\left(\rho\vec{U}\right)+\nabla\cdot\left(\rho\vec{U}\vec{U}\right)=-\nabla P+\nabla\cdot\left(\bar{\bar{\tau}}\right)+\rho\vec{g}, \tag{3}$$

the total energy equation,

$$\frac{\partial}{\partial t}(\rho E)+\nabla\cdot\left(\vec{U}(\rho E+\rho)\right)=\nabla\cdot\left(k\nabla T-h\vec{J}+\left(\bar{\bar{\tau}}\cdot\vec{U}\right)\right), \tag{4}$$

where,

$$E=h-\frac{P}{\rho}+\frac{U^2}{2}, \tag{5}$$

and enthalpy for incompressible flow is

$$h=\int_{T_{\text{ref}}}^{T}C_p dT+\frac{P}{\rho}, \tag{6}$$

The boundary conditions applied to the model are illustrated in Fig. 3. The inlet is treated as a mass-flow-inlet with a prescribed rate of 1.1 g/s at a temperature of 291.1 K, as per experimental conditions. The outlet is given the 'outflow' condition in which no parameters are prescribed.

The edges along which the cone is unrolled are treated with a cyclic-periodic boundary condition to capture the conduction from one side of the cone to the other. The outside wall, front and back edges of the cone are treated as insulated.

The inside wall of the cone is irradiated from the concentrating mirror. The total power deposited into the TR is calculated from Eq. 7.

$$P_{in}=C_{shadow}\cdot C_{reflect}\cdot C_{mask}\cdot A_{mirror}\cdot\overline{\text{DNI}} \tag{7}$$

The average direct normal irradiance ($\overline{\text{DNI}}$), measured in W/m^2, during the experiment is scaled to account for several instrumental factors. We multiply by the area of the mirror with $A_{mirror}=(1.65\text{ m})^2$. Then, we multiply by a masking factor to account for the fact that 35% of the mirror is uniformly covered to reduce the total power for this particular test case, thus

$C_{mask} = 0.35$. Then, the solar-weighted reflectance of the mirror is accounted for with $C_{reflect} = 0.92$. Finally, the TR assembly and support-arm cast a shadow on the mirror which is accounted for by $C_{shadow} = 0.97$. Each of these values is assigned an uncertainty of 1% which ultimately gives us an input power to our model of $P_{in} = 826 \pm 15$ W.

The total power into the TR is assigned by way of a custom heat-flux profile in FLUENT. The heat flux profile comes from previous work using a solar ray-tracing simulation [3]. The results of the ray tracing simulation give the solar intensity as a function of axial depth into the cone. The solar intensity profile is un-rolled into the profile seen in Fig. 4. The profile is normalized such that the total power in is $P_{in} = 826$ W.

3.2. Modeling receiver losses

To determine the scale of losses from the system we begin with simple approximations. To account for radiative losses, we approximate the TR with an isothermal disk with a diameter equal to the entrance diameter. Then we calculate,

$$Q_{rad} = \epsilon\sigma A\left(T_w^4 - T_{sky}^4\right) \tag{8}$$

where $\epsilon = 0.85$ [7], σ is the Stefan–Boltzman constant, A is the aperture-disk area, $T_w = 450$ K and $T_{sky} = 273$ K. Thus, $Q_{rad} \approx 2$ W. Compared to P_{in}, Q_{rad} is low. However, for higher-temperature heat transfer fluid and TR wall temperatures, radiation losses could become significant.

To account for convective losses, we begin by calculating Re for external flow,

$$\mathrm{Re} = \frac{\overline{u} D_{ap}}{\nu} \tag{9}$$

where $\overline{u} = 1.8$ m/s from measurement, $D_{ap} = 38$ mm, and ν is the kinematic viscosity of air evaluated at T_∞. This gives Re $\approx$ 4500. As the temperature of the air increases, the kinematic viscosity increases such that Re decreases. Thus, external flow is in the laminar regime.

Next, the Grashof number is calculated to determine the effect of free convection,

$$\mathrm{Gr} = \frac{g\beta(T_w - T_\infty)D_{ap}^3}{\nu^2} \tag{10}$$

where $\beta \approx 1/T$. Once again, as the air temperature increases, β decreases and ν increases such that Gr decreases.

We calculate the ratio, $\mathrm{Gr}/\mathrm{Re}^2 \leqslant 0.09$ suggesting that free convection could be ignored. However, the direction of the wind is unknown and the air speed inside the cone is likely to be very low if not static. Therefore, free convection is not ignored.

The TR is then approximated once again by an inclined isothermal disk with the dimensions of the aperture plane. We use a correlation equation valid over a large range of Ra (Ra = Gr · Pr) recommended by Churchill and Chu [9]. This correlation is valid for free convection from a vertical or inclined plate by replacing g with $g \cdot cos(\theta), 0 \leqslant \theta \leqslant 60°$.

$$\overline{\mathrm{Nu}} = 0.68 + \frac{0.670 \cdot \mathrm{Ra}^{1/4}}{\left[1 + (0.492/\mathrm{Pr})^{9/16}\right]^{4/9}} \tag{11}$$

This approximation gives Nu $\approx$ 14.5, and therefore, $Q_{conv} \approx 3.5$ W for $0 \leqslant \theta \leqslant 60°$.

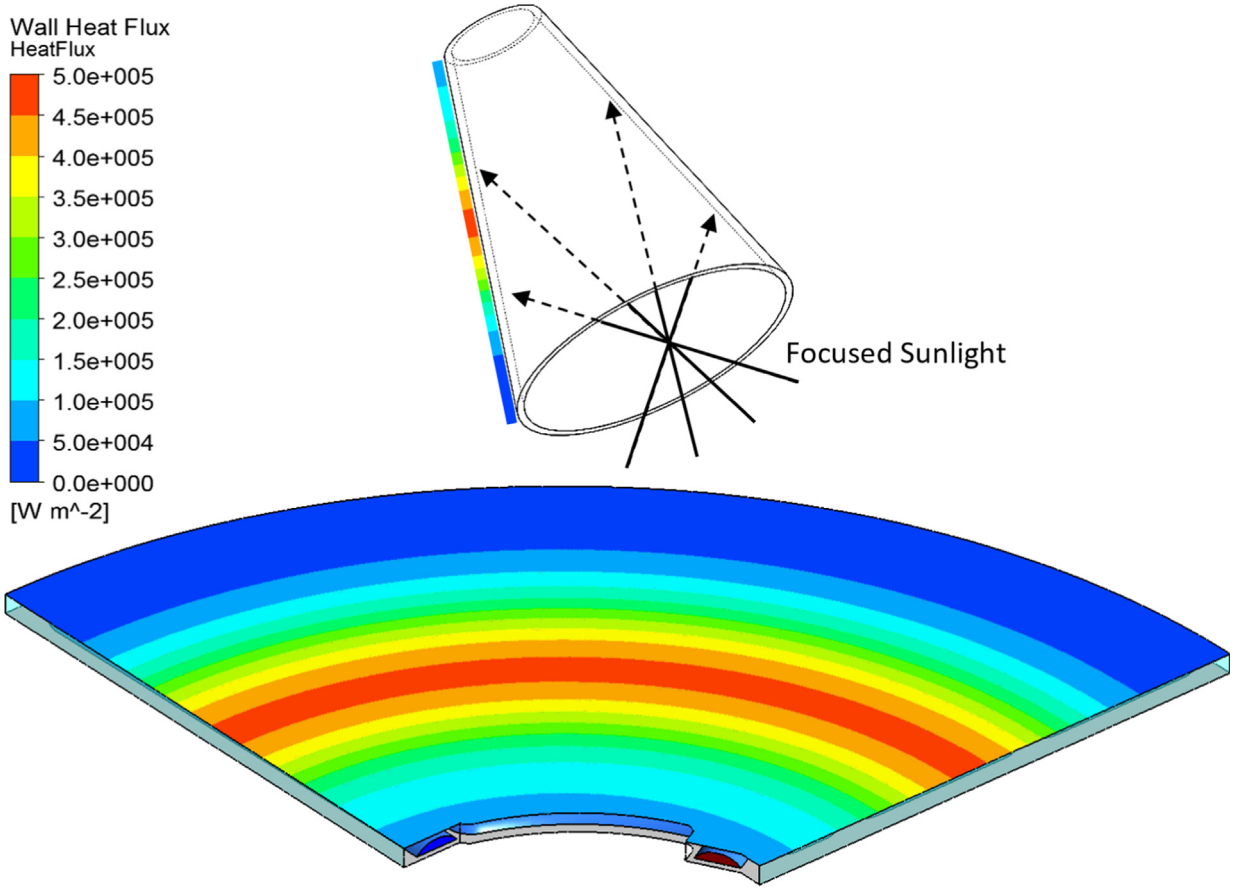

Fig. 4. Solar heat flux mapped onto the unrolled cone.

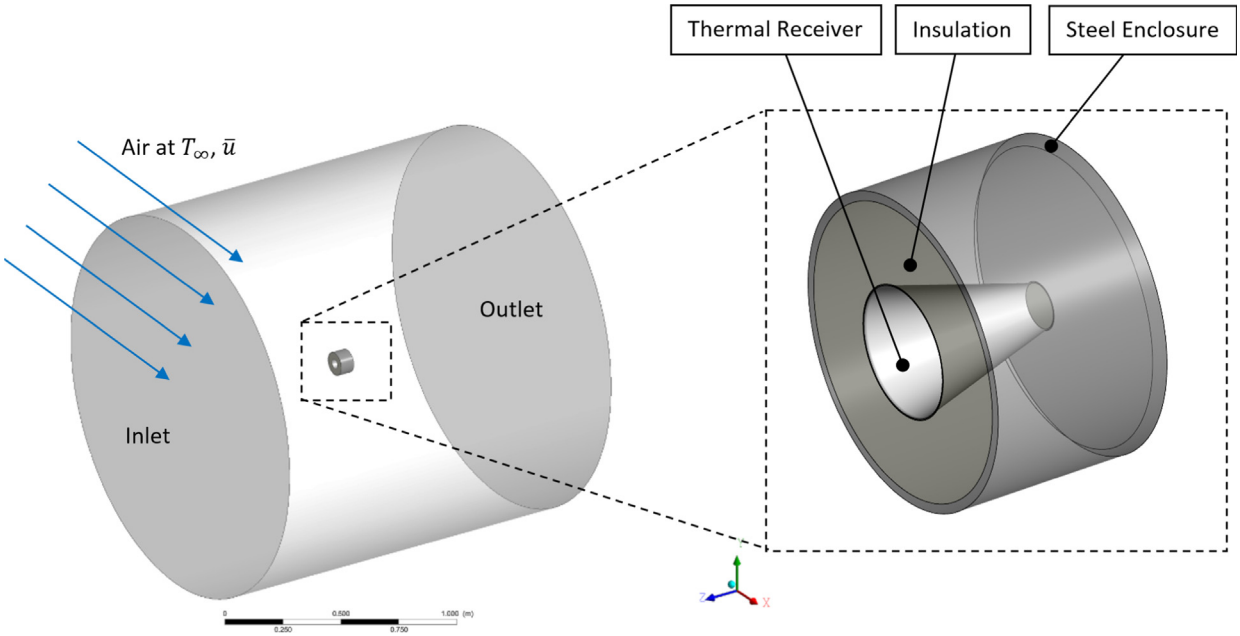

Fig. 5. CFD model used to approximate the heat loss from the TR to the environment.

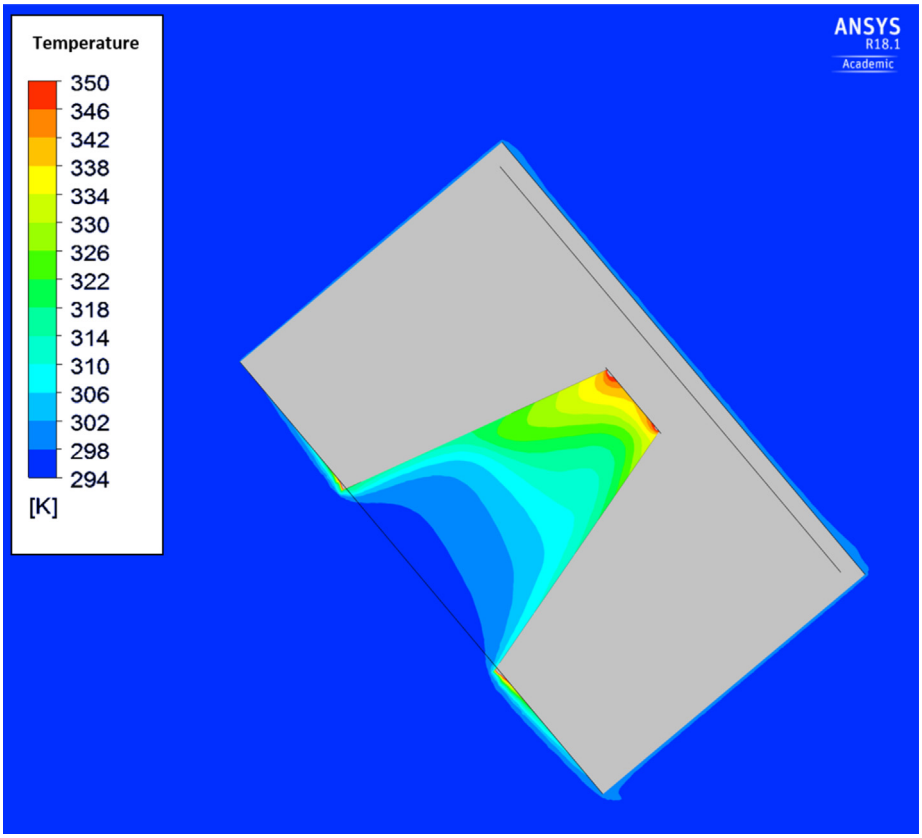

Fig. 6. Heat transfer from TR to the environment. Contours of air temperature of for a mid-plane cross-section of the domain shown in Fig. 5.

This approximation is expected to be an underestimate of the total heat loss due to convection as it does not account for the non-zero ambient wind speed. Therefore, to determine the full convective losses to the environment, we construct an additional CFD model.

The second CFD model, illustrated in Fig. 5, is used to approximate the heat loss from the TR to the environment. The model contains a simplified TR assembly centered in a cylindrical air domain. The assembly consists of an inconel cone surrounded by high-temperature mineral wool insulation and enclosed in a steel case.

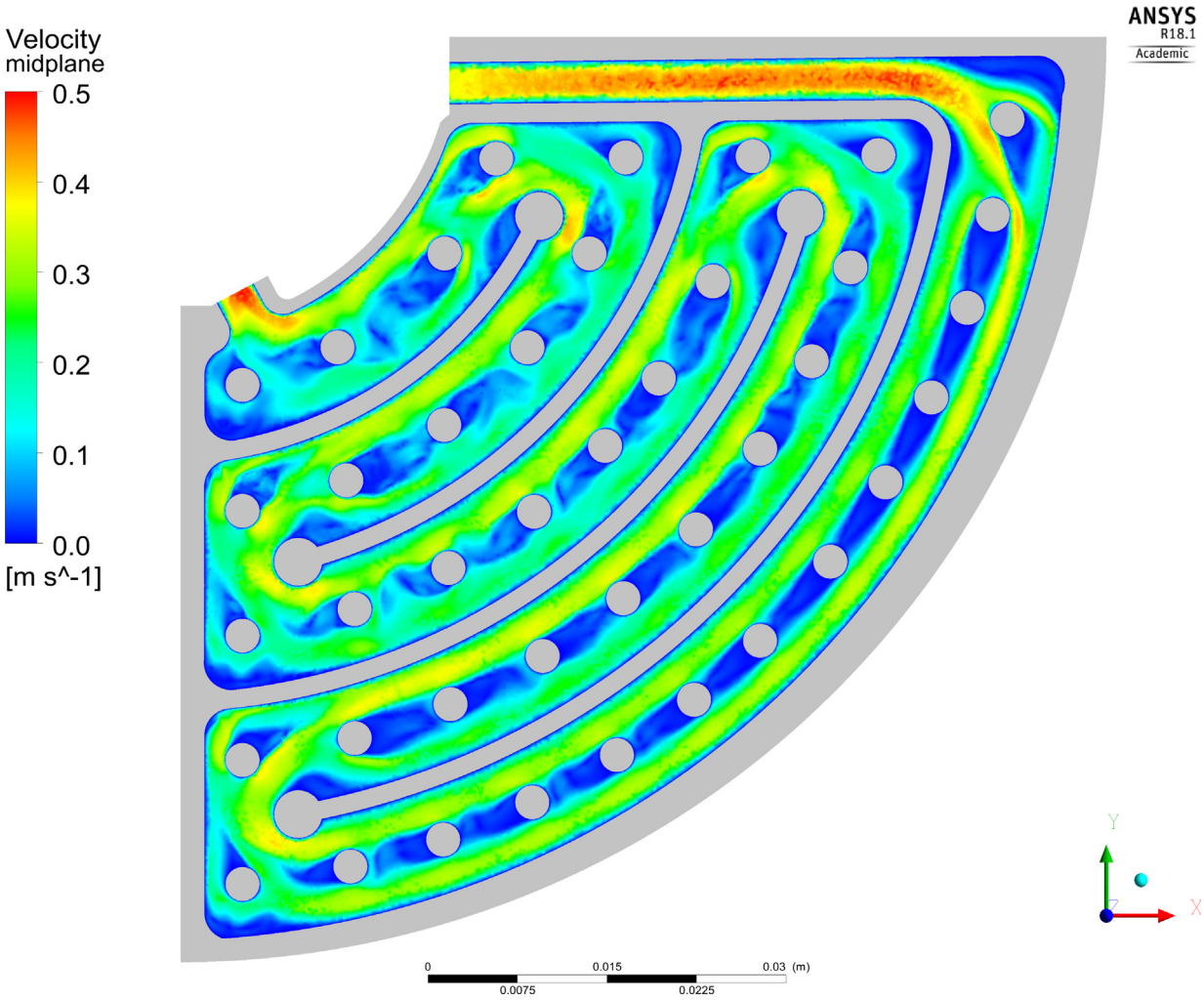

Fig. 7. Fluid velocity at the midplane of the TR.

The receiver assembly without the PV array is similar to cavity-receivers found in other CSP applications. These cavities are known to primarily lose heat due to convection to the surrounding air, especially in the presence of wind normal to the aperture plane [10,11].

The diameter of the surrounding domain is greater than 10 times the diameter of the cone aperture. Previous work found this scale of the cavity with respect to the domain acceptable to avoid boundary effects.

The inside wall of the thermal receiver assembly is treated as isothermal. The prescribed wall temperature, T_w is set to the mean temperature of the inside wall from the TR model described in Section 3.1.

The inlet properties of the air domain were set according to the average measured values during the experiment. The velocity was set to $\overline{u} = 1.8$ m/s, and the inlet temperature was set to $T_\infty = 21.9\ ^\circ$C.

The wind direction is varied to determine an average of the convective losses while the TR is at different positions. Several reports have found that convection from such a cavity is highest when the wind direction is aligned with the cone axis, and minimized when orthogonal to the cone axis [10,11].

To determine an upper bound for convective losses, the wind direction is 'head on' with respect to the TR.

This model achieved a steady-state solution reporting a net loss of $Q_{conv} = 4.5$ W at $\theta = 45^\circ$ from the inside wall of the cone to the environment.

Temperature contours for a cross-section – such that gravity is in the downward direction - of the air domain are shown in Fig. 6. The temperature distribution suggests that heat transfer to the surrounding air is not significant at this scale, and for this temperature range. Although, for a larger cavity at a higher temperature, convective losses could be severe.

4. Results

First we present results from the experiment and both CFD models to demonstrate their validity.

4.1. Model validation

Since conductive, convective and radiative losses each amount to less than 1% of the input power, they can be neglected from the TR model.

The TR model achieved a steady-state solution after approximately 700 iterations. The outlet temperature, measured at the midplane, reported by the model is 206 °C.

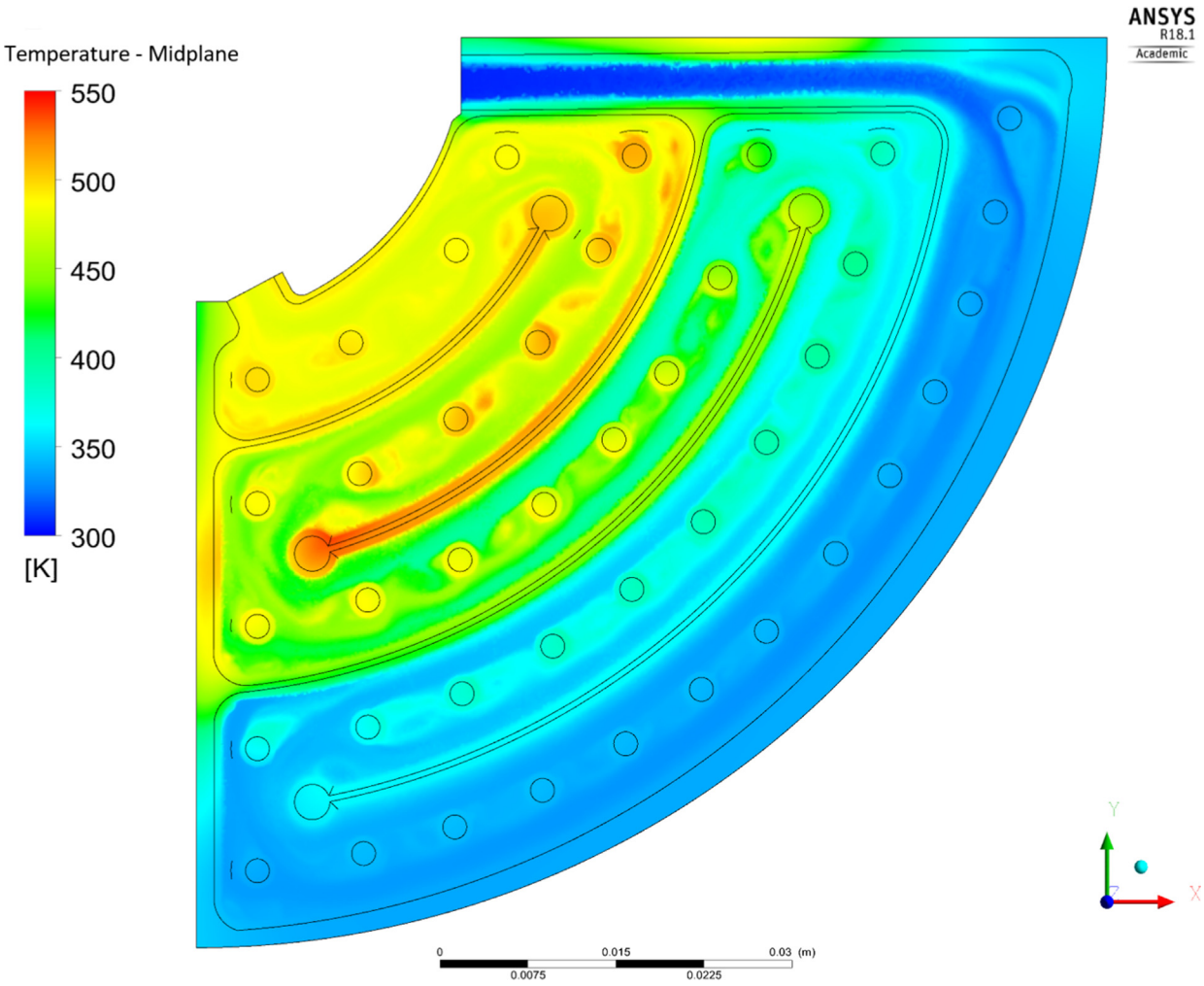

Fig. 8. Temperature at the midplane of the TR. Both the inconel and the fluid are included in this temperature distribution.

4.2. Model results

Contours of velocity at the midplane of the TR model are shown in Fig. 7. The fluid enters the TR in the laminar regime. However, after several passes around the serpentine path, the temperature is sufficiently high to lower the fluid viscosity and create vorticies around the spot-welds. Recall that the operating pressure of the TR is 19 bar to keep the working fluid in the liquid phase.

The temperature of both the inconel and the water at the midplane of the TR are presented in Fig. 8. The temperature of the inconel is strongly coupled to the solar-flux distribution inside the cone, as per Fig. 3. Therefore, the inconel between the third and fourth arcs (when counting from the outside) is highest. This causes a localized hot-spot in the TR near a zone with poor circulation, visible in Fig. 8.

To condense the results of the model, we take the contours of the temperature at the midplane, shown in Fig. 8. We then select the line parallel to the main axis of the cone and coincident with the midpoint of each arc. The temperature distribution is integrated along segments of this path for each of the five arcs. The result is shown in Fig. 9. The mean temperature in Fig. 9 was determined by integrating the temperature along a path parallel to the main axis of the cone. The size of the error-bars in Fig. 9 are indicative of the level of fluid re-circulation occurring for that arc. We can see that the temperature in the initial arc and the final arc have relatively little temperature variation when compared to the middle three arcs. This indicates that by the final arc of the TR the fluid is relatively homogenized.

5. Conclusion and future work

A conical thermoplate heat exchanger which is the central heat exchanger in a novel hybrid solar thermal collector is modeled in this paper. A laminar model is used to predict the results of fluid flow and heat transfer since the majority of the flow is in the laminar regime. However, Re reached values above 2300 within the computational domain and future work will attempt solving the flow field using turbulent models. Key findings include:

- The small scale cavity receiver performance is accurately modeled using a simplified unrolled version for coupled thermofluidic CFD analysis.
- ANSYS-FLUENT calculations were performed in parallel on the HPCC. The computational mesh contains close to 3 million elements. Clock time was on the order of 10 min.
- The computational model predicted HTF exit temperature agrees within 1% of experimental results during steady state operation at 2.5 kW nominal system power.
- Conductive, convective, and radiative losses are modeled using a larger control volume surrounding an isothermal conical receiver, set at the mean receiver inside wall temperature.

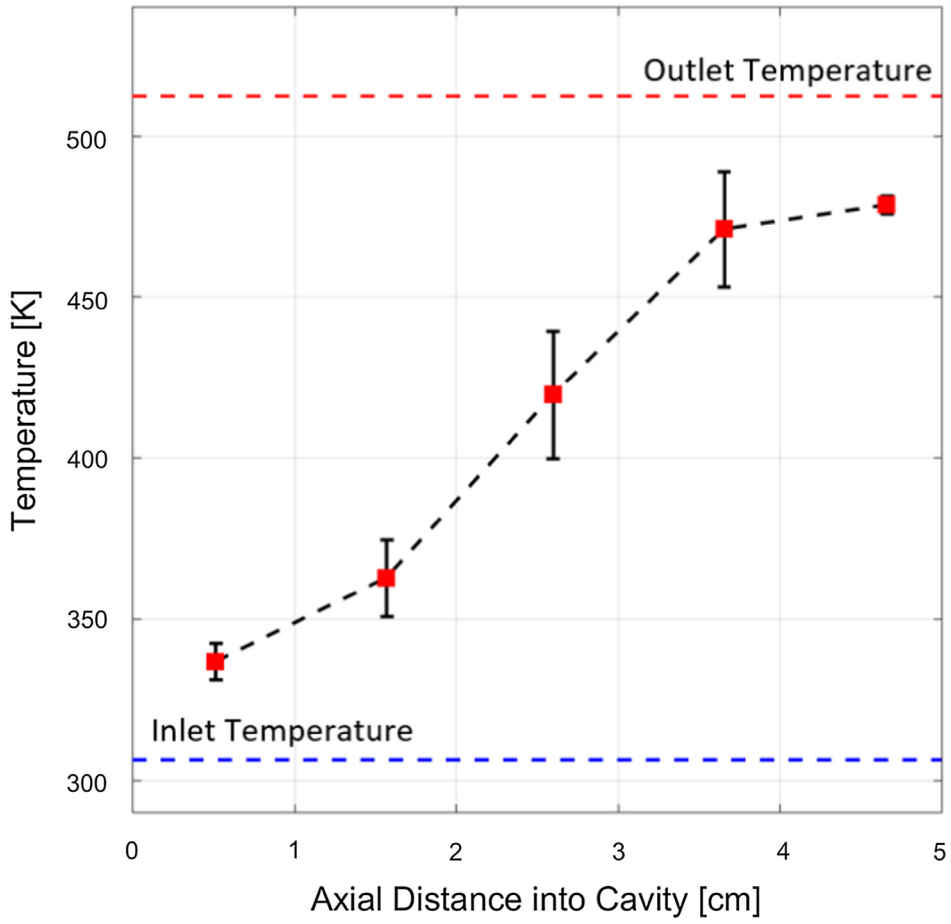

Fig. 9. Mean temperature for each of the five arcs of the serpentine fluid path. The abscissa values are at the midpoint of each arc. Error bars indicate the standard deviation.

Testing and refinement of the receiver design, prototypes, and models are ongoing, including larger aperture designs compatible with higher temperature molten salt operation and variable spot weld geometry for enhanced mixing.

Acknowledgement

The information, data, or work presented herein was funded in part by the Advanced Research Projects Agency - Energy, U.S. Department of Energy, under Award No. DEAR0000473.

References

[1] H.M. Branz, W. Regan, K.J. Gerst, J.B. Borak, E.A. Santori, Hybrid solar converters for maximum exergy and inexpensive dispatchable electricity, Energy Environ. Sci. 8 (11) (2015) 3083–3091.
[2] B.C. Riggs, R. Biedenharn, C. Dougher, Y.V. Ji, Q. Xu, V. Romanin, D.S. Codd, J.M. Zahler, M.D. Escarra, Techno-economic analysis of hybrid PV/T systems for process heat using electricity to subsidize the cost of heat, Appl. Energy 208 (2017) 1370–1378.
[3] Q. Xu, Y. Ji, B. Riggs, A. Ollanik, N. Farrar-Foley, J.H. Ermer, V. Romanin, P. Lynn, D. Codd, M.D. Escarra, A transmissive, spectrum-splitting concentrating photovoltaic module for hybrid photovoltaic-solar thermal energy conversion, Sol. Energy 137 (2016) 585–593.
[4] Y. Ji, Q. Xu, B. Riggs, K. Islam, A. Ollanik, J.H. Ermer, D.D. Krut, V. Romanin, D. Codd, M.D. Escarra, Optical design and validation of an infrared transmissive spectrum splitting concentrator photovoltaic module, IEEE J. Photovolt. 7 (5) (2017) 1469–1478.
[5] Y. Ji, A. Ollanik, N. Farrar-Foley, Q. Xu, L. Madrone, P. Lynn, V. Romanin, D. Codd, M. Escarra, Transmissive spectrum splitting multi-junction solar module for hybrid cpv/csp system, in: 2015 IEEE 42nd Photovoltaic Specialist Conference (PVSC), IEEE, 2015, pp. 1–5.
[6] I. Khalil, R. Hayes, Q. Pratt, C. Spitler, D. Codd, Experimental and numerical modeling of heat transfer in directed thermoplates, Int. J. Heat Mass Transf. 123 (2018) 89–96.
[7] C.K. Ho, A.R. Mahoney, A. Ambrosini, M. Bencomo, A. Hall, T.N. Lambert, Characterization of pyromark 2500 paint for high-temperature solar receivers, J. Sol.Energy Eng. 136 (1) (2014) 014502.
[8] W. Wagner, H.-J. Kretzschmar, Iapws industrial formulation 1997 for the thermodynamic properties of water and steam, International Steam Tables: Properties of Water and Steam Based on the Industrial Formulation IAPWS-IF97 (2008) 7–150.
[9] S.W. Churchill, H.H. Chu, Correlating equations for laminar and turbulent free convection from a vertical plate, Int. J. Heat Mass Transfer 18 (11) (1975) 1323–1329.
[10] R. Jilte, S. Kedare, J. Nayak, Natural convection and radiation heat loss from open cavities of different shapes and sizes used with dish concentrator, Mech. Eng. Res. 3 (1) (2013) 25.
[11] R. Jilte, S. Kedare, J. Nayak, Investigation on convective heat losses from solar cavities under wind conditions, Energy Procedia 57 (2014) 437–446.